



The South Atlantic sub-tropical dipole mode since the last deglaciation and changes in rainfall

Ilana Wainer¹ · Luciana F. Prado² · Myriam Khodri³ · Bette Otto-Bliesner⁴

Received: 2 May 2020 / Accepted: 22 September 2020 / Published online: 29 September 2020
© Springer-Verlag GmbH Germany, part of Springer Nature 2020

Abstract

The South Atlantic subtropical dipole (SASD) has an impact on South American rainfall particular during its negative phase when continental precipitation in the northern part of the continent is enhanced. Relying on a series of single forcing transient simulations since the last deglaciation, we differentiate the relative role of meltwater, orbital, ice-sheets and greenhouse gases on the variability of rainfall in South America and links to the SASD. Results indicate that the meltwater forcing is the predominant driver of SASD variability. Wavelet analysis shows that most of the energy for the SASD at lower frequencies (~5 kyr) comes from the meltwater discharge at cold events such as the Heinrich-1 cooling ~ 17 ka and the Younger-Dryas ~ 12.9 ka. Large rainfall changes in Northeastern Brazil can be attributed to changes in the South Atlantic sea surface temperature latitudinal gradient and South Atlantic Northward heat transport driven by the meltwater discharge.

Keywords South Atlantic subtropical mode · Last deglaciation · South America

1 Introduction

Significant changes in ice sheets and greenhouse gases concentration associated with changes in insolation occurred from the Last Glacial Maximum (~ 22 ka) into Pre-industrial times (~ 1850 Common Era (C.E.)). The warming introduced by the orbital forcing starting at LGM drove the decay of ice-sheets and ice-shelves and the influx of meltwater into the ocean. This process greatly impacted the global distribution of water and heat fluxes which was responsible for changes in the oceans and atmosphere. Of particular interest is that this period was marked by extraordinary changes in the North Atlantic where a series of abrupt cooling and warming events took place (e.g. Heinrich-1 (H1) cooling at ~ 17 ka; Bølling–Allerød (BA) warming at ~ 14.5 ka,

warming and the cooling of the Younger–Dryas (YD) at ~ 12.9 ka).

The cooling events were associated with large input of meltwater from the retreating North Atlantic ice-sheets (He et al. 2013) while the BA warming is sometimes related to a meltwater pulse originating from Antarctica (MWP-1A, Weaver et al. (2003); Marson et al. (2014)). Many of these abrupt changes, revealed in the global and regional patterns of climate evolution, were described by Clark et al. (2012) using a compilation of surface temperature and precipitation proxy-records. Furthermore, modeling studies of the transient climate since the Last Glacial Maximum (Liu et al. 2009; He et al. 2013; Wen et al. 2016) were able to simulate the several major features of the cooling (and warming events) of the deglacial climate evolution, suggesting a good agreement between the model and observations. This is also seen in Wainer et al. (2014); Marson et al. (2016); Tierney (2017).

Finally, the Holocene, sometimes considered a climatic period with no significant changes, has been shown to have very interesting variability. It is considered to have started right after the YD event ~ 11.7 ka (Walker et al. 2019). Because of Northern Hemisphere ice-sheet melt, Ruddiman et al. (2016) discuss that global climate was driven into a warm, somewhat stable, state during the Holocene. O'Brien S, Mayewski PA, Meeker LD, Meese DA, Twickler MS,

✉ Ilana Wainer
wainer@usp.br

¹ Inst. Oceanography, University of São Paulo (IOUSP), São Paulo, Brazil

² Inst. Geosciences, University of Brasilia, Brazil - now at IOUSP, University of São Paulo, São Paulo, Brazil

³ LOCEAN/IRD/IPSL - Sorbonne University, Paris, France

⁴ Climate and Global Dynamics Division, National Center for Atmospheric Research, Boulder, CO 80307, USA

Whitlow S, (1995) discuss millennial-scale climatic shifts in the Greenland Ice Sheet Project v2 ice core record (GISP2). Mayewski et al. (2004) show, using globally distributed records, that there is strong climate variability in the Holocene that is characterized by polar cooling, drying at low latitudes and major atmospheric circulation changes.

1.1 The South Atlantic subtropical dipole mode

The South Atlantic subtropical dipole mode (SASD) is an important mode of low-frequency variability in the South Atlantic and has only recently been subject of investigation. One of the first studies to identify the existence of a persistent sea surface temperature (SST) anomaly dipole structure in the South Atlantic associated to sea level pressure changes was Wainer and Venegas (2002). They used Empirical Orthogonal Function (EOF) and singular value decomposition in their analysis. Other studies such as Morioka et al. (2011); Nnamchi et al. (2011); Wainer et al. (2014) discuss the SASD, where it is presented as the dominant mode of climate variability in the South Atlantic (representing about 24% of the explained variance) and a good indicator for rainfall variability in South America. Morioka et al. (2011, 2012) established the SASD as a dipole-like SST pattern with a northeast-southwest orientation where the positive (negative) phase has negative (positive) anomalies in the northern (southern) portion of the dipole.

From a paleoclimate perspective, Wainer et al. (2014) reconstructed the SASD index for the Holocene using SST proxy-data obtained from two marine sediment cores in each-side of the Tropical-South Atlantic Basin representing the two poles of the SASD. The index was then validated using the simulation results from the (full-forcing) NCAR-TraCE21 transient paleoclimate simulation (Liu et al. 2009) and linked to the proxy-reconstructed SASD-index to evaluate its impact on South American rainfall. The simulation results revealed that for the Holocene the SASD composite difference between positive and negative phases of the index yields a precipitation (PPT) dipole over South America. They show an increase of PPT in the northern part of South America (north of about 15° S, with maximum values in the northeast region of Brazil) and decrease south of that associated with the negative phase of the SASD-mode of variability (when the NE pole is positive and the SW pole is negative).

The relationship between Tropical-South Atlantic SST variability and rainfall over African and South American rainfall is not new. For example, the studies of (Moura and Shukla 1981; Servain 1991; Wainer and Soares 1997; Hastenrath 2012) among others, all related changes in Tropical SST with the migration of the Intertropical Convergence Zone (ITCZ) and rainfall in Brazil, particularly in its Northeast region (NEB). These changes in rainfall

were also associated with the interhemispheric SST-gradient that connects both sides of the equator in the tropical Atlantic Ocean. The ITCZ is the furthest south in MAM when Northeast Brazil (NEB) experiences its rainy season. MAM is the season when the SASD is negative, so the Northeast (NE) pole of the SASD overlaps with the Tropical South Atlantic pole of the interhemispheric SST mode (also referred to as the Atlantic Meridional Mode, AMM). This mode has a north-south dipole-like asymmetric pattern with positive/negative SST anomalies on either side of the Equator. The warmer (cooler) pole is associated with weakened (stronger) winds (Deser et al. 2010).

Haug et al. (2001) discuss Holocene drier conditions in the equatorial region of South America. Wetter conditions observed in central-eastern and southeastern Brazil are mentioned in Cheng et al. (2009); Strikis et al. (2015). Furthermore, Baker and Fritz (2015) results are consistent with this idea of the influence of the SASD on South American PPT. They discuss that Tropical-South Atlantic SST and air-sea interactions can have an impact on the climate related rainfall changes in South America from seasonal to millennial and multi-millennial (orbital) time-scales.

The SASD and the AMM climate modes explain many of the links between the tropical Atlantic observed variability and the subtropics. However, the time-scales of these Tropical and Subtropical interactions and their influence on continental rainfall variability is still the subject of scientific debate. In order to improve our understanding of the relationship between changes across different climates of Atlantic SST with PPT in South America, and their relationship with the cold events of the Northern Hemisphere, we examine the full forcing and single forcing results from the NCAR-TraCE21k transient simulation starting at the Last Glacial Maximum (LGM, ~ 22 ka) to pre-industrial times (Liu et al. 2009; He et al. 2013; Buizert et al. 2018). This becomes relevant because the NCAR-TraCE21k simulation incorporates meltwater flux from the retreat of the ice sheets since the LGM into the Holocene.

The present-day spatial pattern of the SASD was established approximately at Mid-to-Late Holocene (~5.5 ka) when there was no more meltwater flux from the high latitudes. The single forcing transient simulations allow us to follow the evolution of the SASD since the last deglaciation and its impact on Northeast Brazil (NEB) rainfall as a response to the individual (natural) forcings. Consequently, we investigate the impacts of the deglacial freshwater discharge assuming contributions from both hemispheres, on the distribution of SST, PPT and heat transport for the Tropical-South Atlantic Ocean. In other words, this paper addresses how the SASD and its influence on NEB rainfall has changed since the LGM as a response to the prescribed MWF.

2 Data and methods

In this study we use the simulation results of the *Transient Climate Evolution over the last 21,000 years* (TraCE-21k) (Liu et al. 2009; He et al. 2013). The full forcing simulation includes transient greenhouse gases concentration, orbital changes, prescribed meltwater flux changes, ice sheets extent and topography, and changing paleogeography as sea level changes from LGM to modern levels.

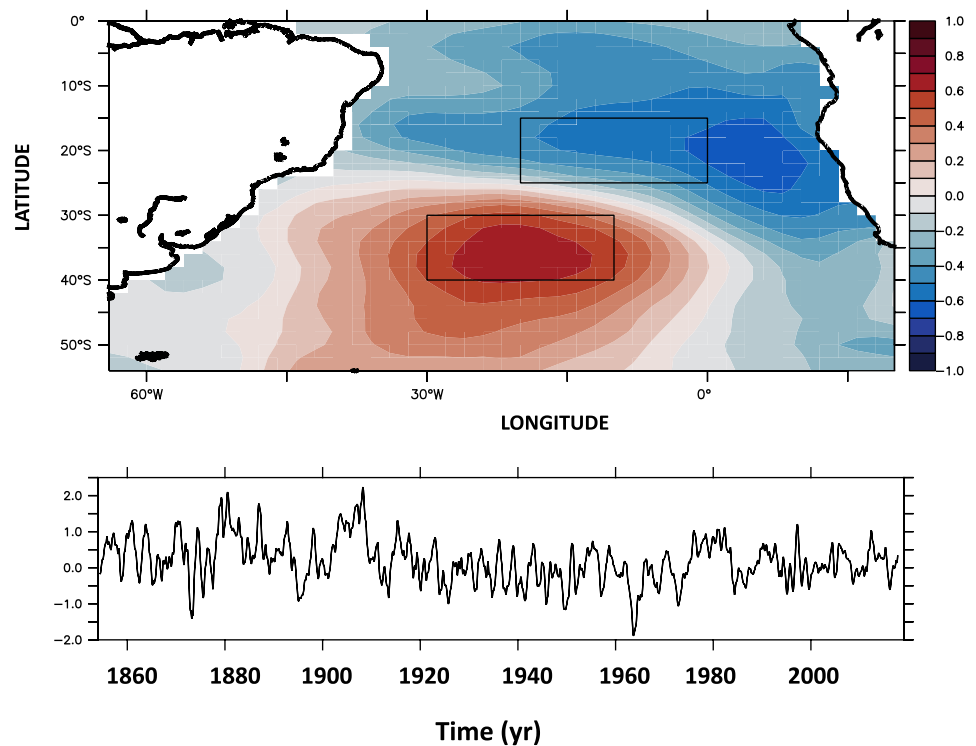
The TraCE-21k model simulations were performed with the coupled ocean-atmosphere-sea ice-land surface climate model from the National Center for Atmospheric Research, the Community Climate System Model version 3 (NCAR-CCSM3, Collins et al. (2006) starting at the Last Glacial Maximum (LGM, 21 ka) into pre-industrial times (PI, 0 ka). The horizontal resolution is approximately 3.75° (T31, Yeager et al. (2006)). Initial conditions were LGM reconstructions Otto-Bliesner et al. (2006). The varying concentrations of greenhouse gases (CO_2 , CH_4 and N_2O) were adopted from Joos and Spahni (2008). The coastlines and ice sheets volume variability followed ICE-5G database Peltier (2004). The orbital parameters at 21 ka (Berger 1978) are used to determine the total solar flux. The simulation includes meltwater fluxes He (2011) from Southern and Northern Hemisphere sources that were added to the ocean model surface freshwater flux. Location and intensity of the meltwater were chosen as a function of known proxy records values (He 2011). Full details of

the boundary and initial conditions can be found on the TraCE-21k homepage: www.cgd.ucar.edu/ccr/TraCE. It is important to note that TraCE-21k simulation results have already been shown to be consistent with many proxy-records and climate dynamics associated with deglacial climate change (e.g. Liu et al. 2009, 2012; Marson et al. 2014; Wainer et al. 2014; Wen et al. 2016).

We analyzed five simulations within the TraCE-21k framework. The first includes all the forcings (hereafter referred to as FULL). The other four are single forcing sensitivity simulations where greenhouse gases (GHG), NH meltwater flux (MWF), continental ice sheets (ICE) and orbital forcing (ORB) are individually allowed to vary in transient simulation while the other forcings are maintained fixed at their 19 ka values. These simulation results are readily obtained from the Earth System Grid (www.earthsystemgrid.org).

The SASD-index can be obtained either using EOF analysis, where the SASD represents the 1st EOF of the SST anomalies in the South Atlantic, or by calculating directly the difference between SST anomalies averaged in its South-western pole (SW: 10°W – 30°W ; 30°S – 40°S) minus those averaged for the Northeastern pole (NE: 0°E – 20°W ; 15°S – 25°S) (Morioka et al. 2011). Here we adopt the latter. The spatial structure of the SASD mode is obtained by the correlation between the calculated SASD-index (differences between SW and NE poles, where the averaging areas are the rectangles in Fig. 1) onto the background SST field where the global mean was subtracted.

Fig. 1 Spatial structure of the SASD mode (top), obtained with reconstructed SST anomalies, based on observations, from NOAA-ERSSTv5 and the SASD-index time series (bottom) which is the difference between the SST anomalies averaged for the SW pole and the NE pole. The boxes indicate the areas of NE and SW SASD poles



The positive (negative) phase of the SASD has negative (positive) anomalies in the NE pole and positive (negative) anomalies in the SW pole and vice-versa for the negative phase. It was shown to be linked to changes in South American precipitation (PPT) (Taschetto and Wainer 2008; Wainer and Venegas 2002; Wainer et al. 2014). For reference, the observed spatial structure of the SASD mode, obtained from the monthly Extended Reconstructed SST data-set, NOAA-ERSSTv5 (Huang et al., 2017) from 1850–2010 is shown in Fig. 1 (top) and the SASD-index (i.e. SW–NE) time series is shown in Fig. 1 (bottom). It should be noted that the pattern correlation between the SASD spatial distribution for the NOAA-ERSSTv5 data set, obtained with both methods (EOF-based and Index-based, shown in Figure S1 in the supplementary material) was calculated in order to better quantify the degree of resemblance. Results indicate that both patterns have an association of 0.799 at 99% confidence level.

3 Results and discussion

Our starting point is the relationship between the SASD and PPT over South America (c.f. Wainer et al. 2014) since the last deglaciation. Changes in rainfall for the Holocene were related to the phase of the SASD-mode showing that the increase/decrease of rainfall was associated with the negative/positive SASD phase. The next step is to look at the evolution of the SASD taking into account the relative importance of each of the forcings (i.e. MWF, ORB, GHG and ICE) and the associated impacts on South American rainfall.

We chose to analyze the SASD spatial pattern by first obtaining the SASD-index as defined by Morioka et al. (2011, 2012) and then regressing the South Atlantic SST onto this index. Using the same set of TraCE-21k full forcing simulations, Wainer et al. (2014) compare for the Holocene different definitions of the SASD index. They consider the SASD index obtained as in Morioka et al. (2011), the SASD index from EOF and the SASD index reconstructed from proxy data. Their results show that the correlation (95% confidence level) between SASD-rec (from proxy) and simulated SASD-avg (index based) is 0.79 while that between SASD index from EOF and SASD-avg is 0.7.

Changes of the SASD spatial structure (and relationship to NEB rainfall) are investigated for five climatic periods as defined in Marson et al. (2014), according to the timing and duration of the prescribed meltwater fluxes. These are Heinrich event 1 (H1, 19 ka–14.67 ka), Abrupt Bølling–Allerød warming and Meltwater Pulse 1-A (BA/MWP-1A, 14.67 ka–13.85 ka); Younger Dryas (YD, 12.9 ka–11.3 ka), Early-Holocene (EHOL, 11.3 ka–6 ka) and Late-Holocene (LHOL, 6 ka–0 ka). The SASD spatial pattern displayed in Fig. 2 for

the FULL simulation results were obtained by regressing the South Atlantic SST onto this index.

The SASD-index time series for all the single forcing experiments are presented in Fig. 3. These help to understand what is driving the SASD variability since the last deglaciation. It can be seen that for the results for the FULL simulation, the South Atlantic (SA) does not display the characteristic dipole pattern of the SASD (cf. Fig. 1) for H1 (Fig. 2a). In fact, it shows that the whole South Atlantic is negative, which combined with the negative SASD-index for the period (black curve in Fig. 3) suggests that the SA basin was warmer. This is consistent with the bipolar sea-saw concept in which the cooling events of the North Atlantic, associated with meltwater events, impact the overturning circulation which in turn lead to the warming of the South Atlantic thus enhancing rainfall in NEB (Mulitza et al. 2017).

For the BA/MWP1-A (during about ~ 800 years, Fig. 2b) a very weak dipole is beginning to be configured, most likely associated with the abrupt Northern Hemisphere warming of BA and the impact of MWP1-A, both which contribute to the spreading of North Atlantic Deep Water (NADW) into the South Atlantic, as discussed in Marson et al. (2014). At YD (Fig. 2c) there is a similar dipole structure that intensifies with a negative area embedded within the SW pole (west of 30° W between 40° S and 30° S). This negative anomaly is located well within the Brazil–Malvinas Confluence Region, probably related to excursions of the warm western-boundary Brazil current.

The dipole structure seen in Fig. 2b–d does not have the characteristic SW–NE tilt of the observations, but this starts developing as the meltwater discharge weakens. By the Late Holocene, no meltwater discharge occurred (Fig. 2e) and the spatial structure of the SASD is very similar to the observed in Fig. 1. The SASD being negative means that the SW pole is cooler while the NE pole (closer to the equator) is warmer. Therefore, when there are active meltwater pulses, the South Atlantic is mostly warm (negative SASD).

Observation of the evolution of the standardized SASD-index in Fig. 3 where each individual forcing experiment is considered, reveals that the meltwater forcing (MWF-red curve in Fig. 3) has the largest impact with respect to the variability of the full-forcing SASD-index (FULL -black curve, Fig. 3) particularly for H1 and YD where the SASD-index is below -1.5 standard deviations. MWF is still important at 8.5 ka however, GHG (blue curve in Fig. 3) and ORB (green curve in Fig. 3) also seem to contribute for the negative peak in the FULL SASD-index variability.

Wavelet analysis Wavelet analysis is a powerful complementary tool to examine the SASD signal characteristics and patterns over the past deglaciation and the relative influence of each of the natural forcings. With this analysis we can obtain insights into the interplay of the lower and higher

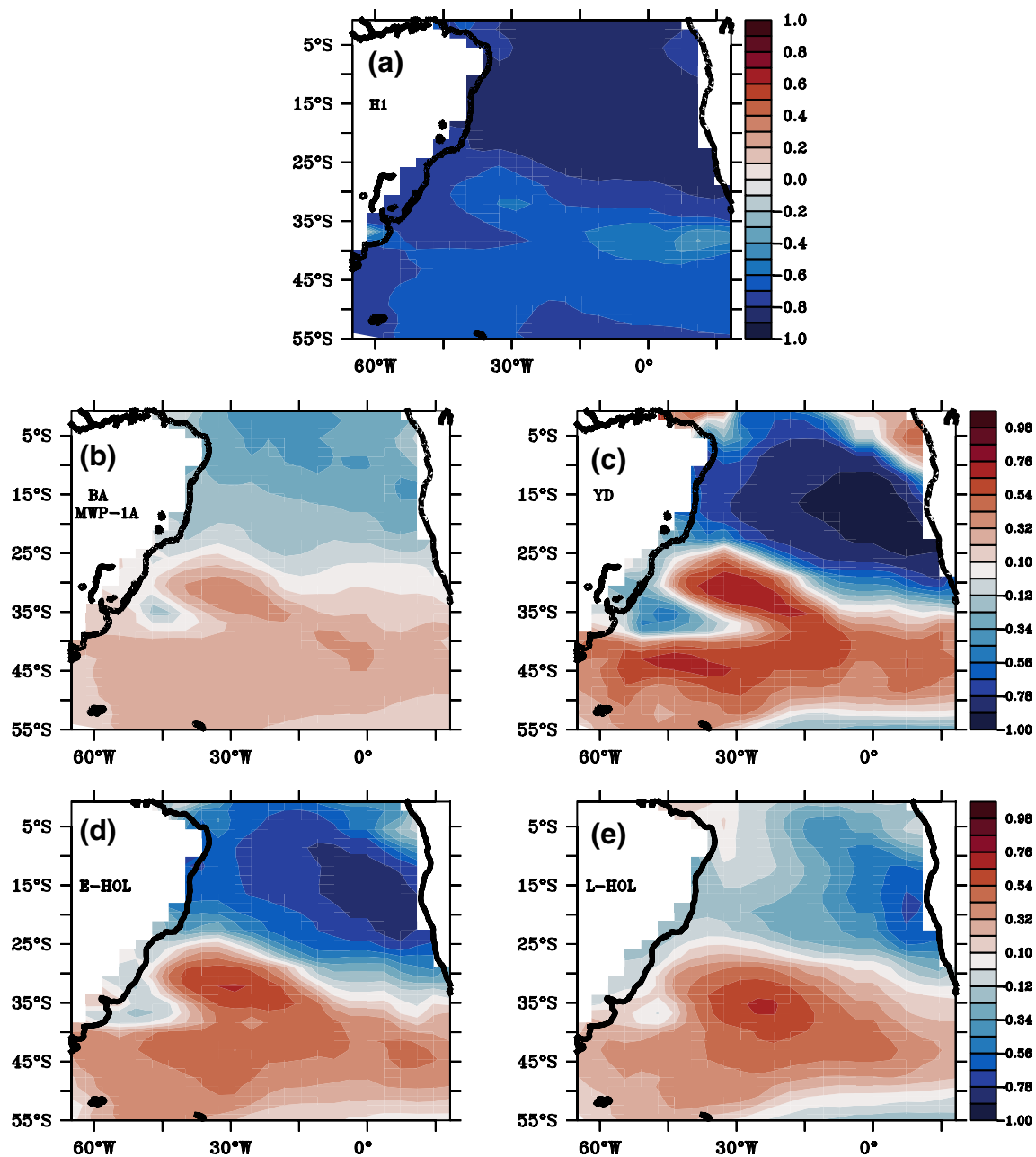


Fig. 2 SASD spatial structure for the TraCE-21k full forcing simulation results considering five different climatic periods defined by the prescribed meltwater fluxes as in He (2011) and Marson et al. (2014): **a** H1 (19 ka–14.67 ka); **b** BA/MWP1-A (14.67 ka–13.85 ka); **c** YD

12.9 ka–11.3 ka); **d** Early Holocene (11.3 ka–6 ka); **e** Late Holocene (6 ka–0), where recovered spatial pattern is very similar to that of the spatial structure of the SASD-mode in the ERSST observations (c.f. Fig. 1)

time-scales of variability in the time-varying spectral content of the SASD-index and see how it relates to source mechanisms. Here we use a Morlet wave function for our continuous wavelet transform. The specific approach follows that outlined in Torrence and Compo (1998).

Figure 4 shows the wavelet power levels for the SASD-index (c.f. Fig. 3) as a function of period for the integration time for all simulations. A clear separation in frequency

and power is observed between the wavelet spectrum for the FULL and MWF relative to the others. For FULL and MWF (Fig. 4a, b) the highest power is confined to the lower periods (centered around ~ 5 kyrs) from the LGM-H1 to about 6 K when the meltwater discharge comes to a halt. We see a spreading of the energy from lower into higher periods around 14 kyr, particularly for the MWF wavelet spectrum. This is most likely an effect of the BA/MWP1-A

Fig. 3 Time series of the standardized SASD-index for each of the TraCE-21k transient runs considered: Full forcing (FULL-black); Meltwater flux only (MWF-red); orbital (ORB-green); greenhouse gas (GHG-blue) and ice-sheets (ICE-cyan)

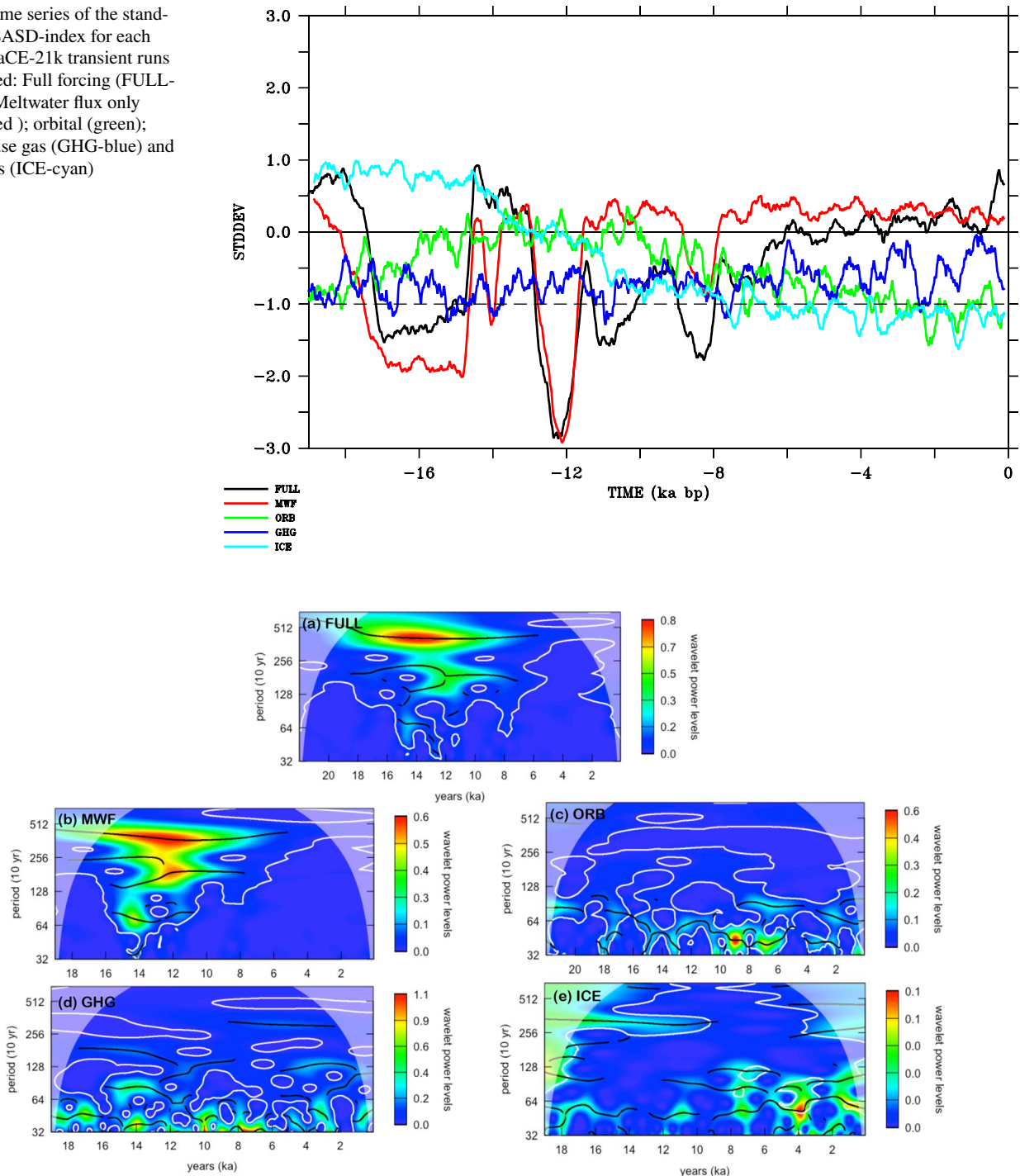


Fig. 4 Wavelet power levels for the SASD-index (c.f. Fig. 3) as a function of period for the integration time considering the simulation results of **a** FULL; **b** MWF; **c** ORB; **d** GHG and **e** ICE

events. It should be noted that the power leakage from higher to lower periods in FULL and MWF wavelet spectra reveals the abrupt aspect of meltwater pulses.

The peaks with maximum power in the FULL and MWF simulations correspond to the meltwater pulses related to Heinrich 1, Younger Dryas, and 8.2 ka events. In these

events, power spreads from higher to lower frequencies, and presents a “funnel shape”. A “funnel shape” in the wavelet spectrum is a large amplitude artifact that occurs when there is a sharp discontinuity in the signal, revealing a sudden, marked change in the time series (e.g. Addison (2018)). Thus, both FULL and MWF spectra do not reveal

a specific periodicity at 5000 years, but an artifact related to the sharp discontinuities in the signal correspondent to the meltwater pulses.

Examination of the SASD-index wavelet spectrum for the ORB and GHG simulation results (Fig. 4c, d) reveal that there is no energy at periods lower than ~ 600 kyrs. The wavelet spectrum for ORB has the highest energy centered at about ~ 400 yrs, between 10 ka and 6 ka while the wavelet spectrum for the SASD-index for the GHG simulation results has power throughout the simulation at most periods higher than ~ 400 years, with a brief period with no signal at ~ 2 kyrs after which, the signal recovers. The power in the wavelet spectrum for the ICE simulation results is about 50%–60% less than the other experiments and most of it is seen after ~ 7 kyrs into PI where there is energy in the periods higher than ~ 700 years with the highest value at 4 ka.

The next question is if the extreme changes in SASD-index impact on the NEB rainfall for each of the periods considered, and why. First, we regress the South Atlantic SST field onto the NEB precipitation index (PPT averaged for Northeastern Brazil) which is shown in Fig. 5. The resulting spatial patterns for each period are very similar to the ones in Fig. 2 which means that the spatial structure of the SASD are recovered, but with opposite signs, which indicates the strong relationship between this mode of variability and continental precipitation in Northeast Brazil as already shown by Wainer et al. (2014) for the Holocene. The difference in sign of the spatial pattern occurs because an increase in rainfall is associated with warmer NE pole temperatures which are connected to the negative phase of the SASD-index. The warmer South Atlantic brings the ITCZ further South which is responsible for enhanced NEB rainfall, consistent with McGee et al. (2014).

Previous studies using PPT proxy records from speleothems (Stríkis et al. 2015, 2018) and marine sediment records (Mulitza et al. 2017) show that there is a substantial strengthening of the continental rainfall during H1. Mulitza et al. (2017) also discuss the increase in rainfall for YD. Both studies discuss the importance of the relationship between AMOC strength and SST difference associated with changes in heat transport as impacting the rainfall in South America.

In order to inspect the relationship between SASD, NEB, SST-gradient and heat transport, we plot the standardized time-series for the NEB-index (defined here as the averaged precipitation between 45° W– 35° W, Eq– 10° S) together with the SASD-index, South Atlantic SST gradient (SATL-SSTgrad, which is equivalent to the SASD and included here to reinforce its relationship to the other parameters. It is defined as $\frac{\partial T}{\partial y}$ between 35° S - EQ) and the South Atlantic Northward Heat transport (SATL-NHEAT,

between 35° S-EQ) in Fig. 6. It is seen that an increase in NEB rainfall is strongly linked to a negative SASD. In fact, correlation of the NEB index with the SASD-index is -0.88 (significant to 95%). This relationship in turn can be explained by the increase in the southward SST gradient and northward heat transport.

The anti-phase relationship between NEB rainfall and the SASD (c.f. Fig. 6) is robust in all single forcing runs, but changes considerably in magnitude. When only the meltwater flux is allowed to vary (MWF runs) the correlation between NEB and SASD increases to -0.92 at 95% significance, confirming the key role that meltwater discharge represents. The correlation between NEB and the SASD decreases considerably for GHG (-0.3 at 95% significance) and ORB (-0.4 at 95% significance). For ICE, the largest changes in variability are from 19 ka to about 11 ka (correlation of -0.9) after which the variability for NEB and SASD is very near 0.

Further investigation of Fig. 6 shows that NEB-ppt starts to decrease in the Holocene and after the 8.2 k event becomes more negative while the SASD index, becomes more stable (i.e. does not exhibit any specific trend.) The SST-gradient increases from early-to-late Holocene indicating a warming towards the North Atlantic consistent with the reduction in continental NEB rainfall.

The evolution of the zonally averaged Atlantic northward heat transport anomaly, in response to the prescribed meltwater flux for the full forcing simulation (FULL), can be understood by examining the latitude vs. time diagram presented in Fig. 7a. The Equator is marked with a solid line. Dashed boxes highlight the occurrence of meltwater inflow. The negative (blue) values of the heat transport means that the South Atlantic is receiving more heat. This is noted in the latitude vs. time distribution of the zonally averaged Atlantic SST-gradient (Fig. 7b). When there is inflow of meltwater associated with the NH cooling events, the SST-gradient is southward (negative) which means that temperatures are increasing southward. Note that for the BA warming, and from the mid-Holocene to PI the northward heat transport anomaly is positive (indicating cooling of the South and warming of the North Atlantic) while the SST-gradient becomes positive meaning it is increasing northward (c.f. Fig. 7). Therefore, looking back at Fig. 6 it becomes clear that the meltwater discharge warms the South Atlantic by weakening the heat transport which shifts the ITCZ south and brings more continental rainfall for NEB.

Changes in the AMOC could contribute to anomalous heating of one hemisphere over the other, thus shifting the strength and spatial distribution of the mode. This is to say, with meltwater events there is a decrease in the AMOC, decrease in the northward heat transport which would impact on the SST anomalies with differential warming between the Northeastern and Southwestern Atlantic affecting the SASD.

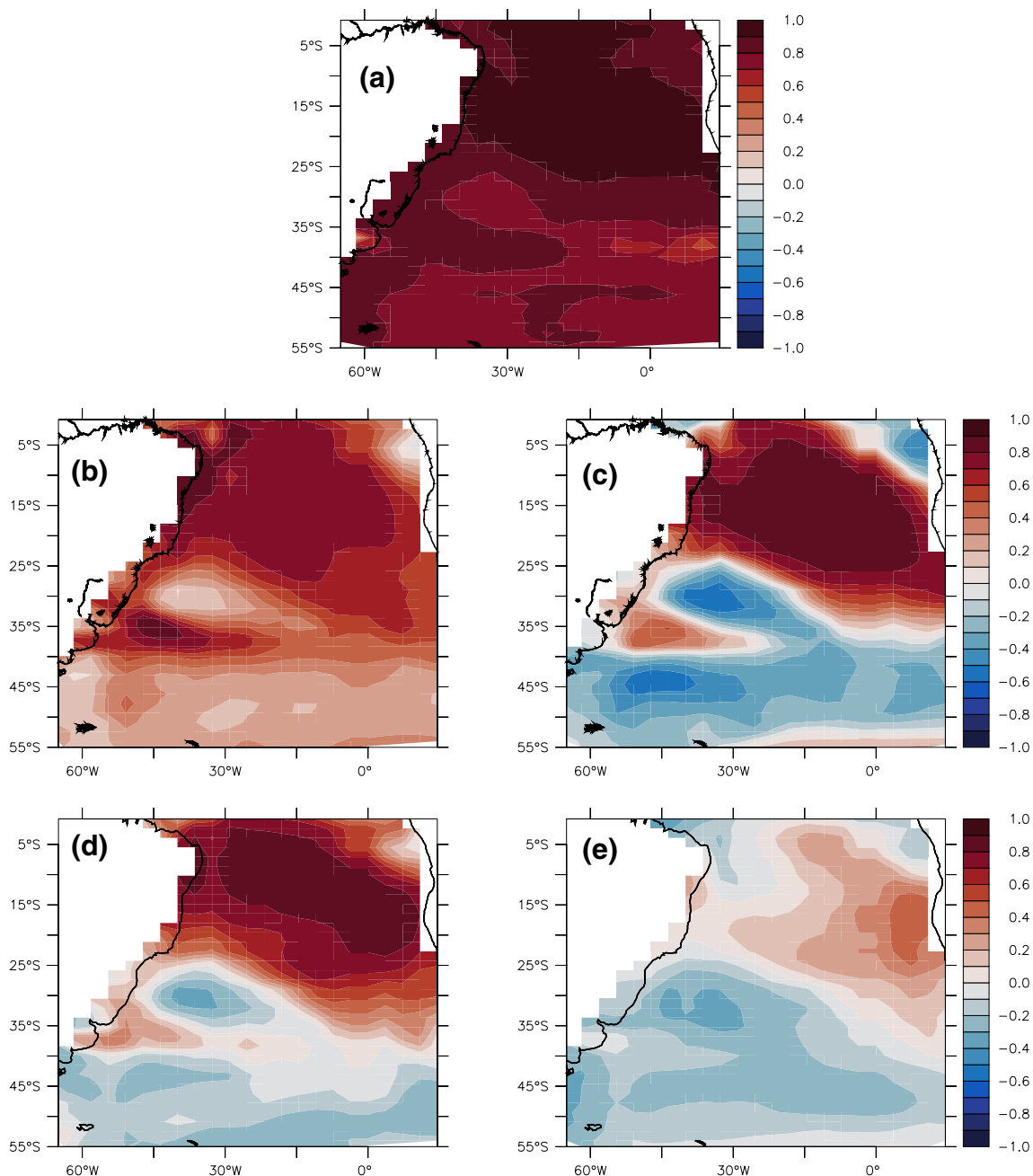


Fig. 5 South Atlantic SST regressed onto NEB precipitation index (PPT averaged for Northeastern Brazil) considering five different climatic periods defined by the prescribed meltwater fluxes as in He (2011) and Marson et al. (2014): **a** H1 (19 ka–14.67 ka); **b** BA/

MWP1-A (14.67 ka–13.85 ka); **c** YD 12.9 ka–11.3 ka); **d** Early Holocene (11.3 ka–6 ka); **e** Late Holocene (6 ka–0). The recovered spatial pattern is very similar to that of the spatial structure of the SASD-mode

Green et al. (2017) and more recently Moreno-Chamarro et al. (2020) find that the ocean (i.e. AMOC) play a significant role in modulating the ITCZ position, where it is biased north for a warmer North Atlantic. The authors discuss the relationship between meridional SST gradients and the ITCZ position across a large range of timescales. They also point out, consistent with this study that paleoclimate proxy records suggest strong NH cooling is linked to a southward

shift of ITCZ during Heinrich and Dansgaard–Oeschger events. In fact, the planktonic foraminifera assemblages analysis of Portillo-Ramos et al. (2017) support the idea of ITCZ shifts to the south for reduced AMOC and accompanying weakened cross-equatorial oceanic meridional heat transport

Lastly, to show the impact of the SASD climate mode of variability impact on the PPT field, we show the

Fig. 6 Standardized time-series of SASD-index (red), NEB-index (black), South Atlantic SST gradient (SATL-SSTgrad, blue) and South Atlantic Northward heat transport (SATL-NHEAT, green).

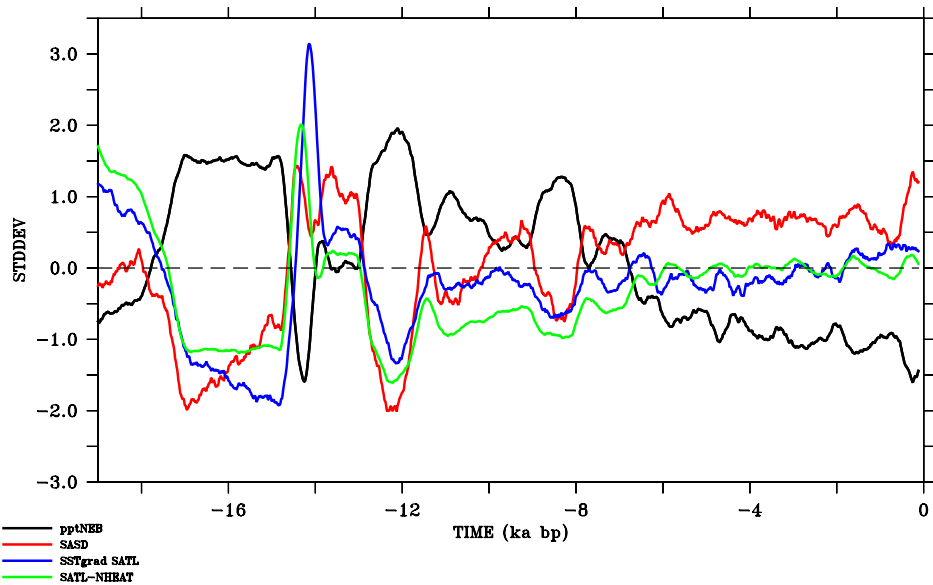
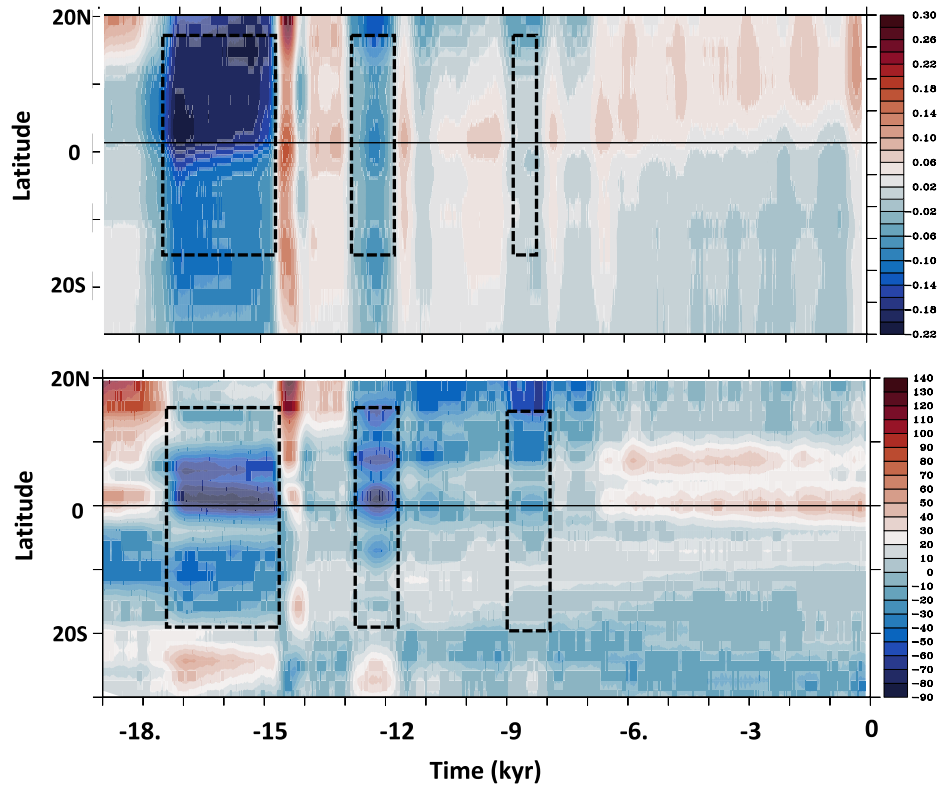


Fig. 7 Time-Latitude diagram of the **a** zonally averaged Atlantic northward heat transport (PW) and **b** zonally averaged SST-gradient ($^{\circ}\text{C}/\text{Lat}$)* $1\text{e-}8$. Black boxes marks the Northern Hemisphere cold events associated with the prescribed meltwater. Negative values indicate weakening of the northward heat transport **a** contributing for the warming of the South Atlantic (**b**, SST gradient increasing southward) except for the BA warming period ($\sim 14\text{ka}$) and from the mid-Holocene into Pre-Industrial times ($\sim 6\text{ka-}0$).



regressions of the PPT for each of the climatic period since the last deglaciation onto SASD-index, in Fig. 8. It is clear that there is an increase in PPT associated with the regions with warmer temperatures, with the spatial structure varying accordingly to the intensity of the SASD mode (c.f. Fig. 2) that changes mostly because of the prescribed meltwater discharge. The pattern that emerges is

of enhanced rainfall in the Northern portion of the South Atlantic domain with intensified continental rainfall north of 20 S and decreased rainfall to the south which is intensified for H1 and YD (Fig. 8a, c). By the late Holocene (Fig. 8e), the pattern is less intense with enhanced rainfall mostly over the ocean north of 10 S west of 0W and north of 20 S east of that.

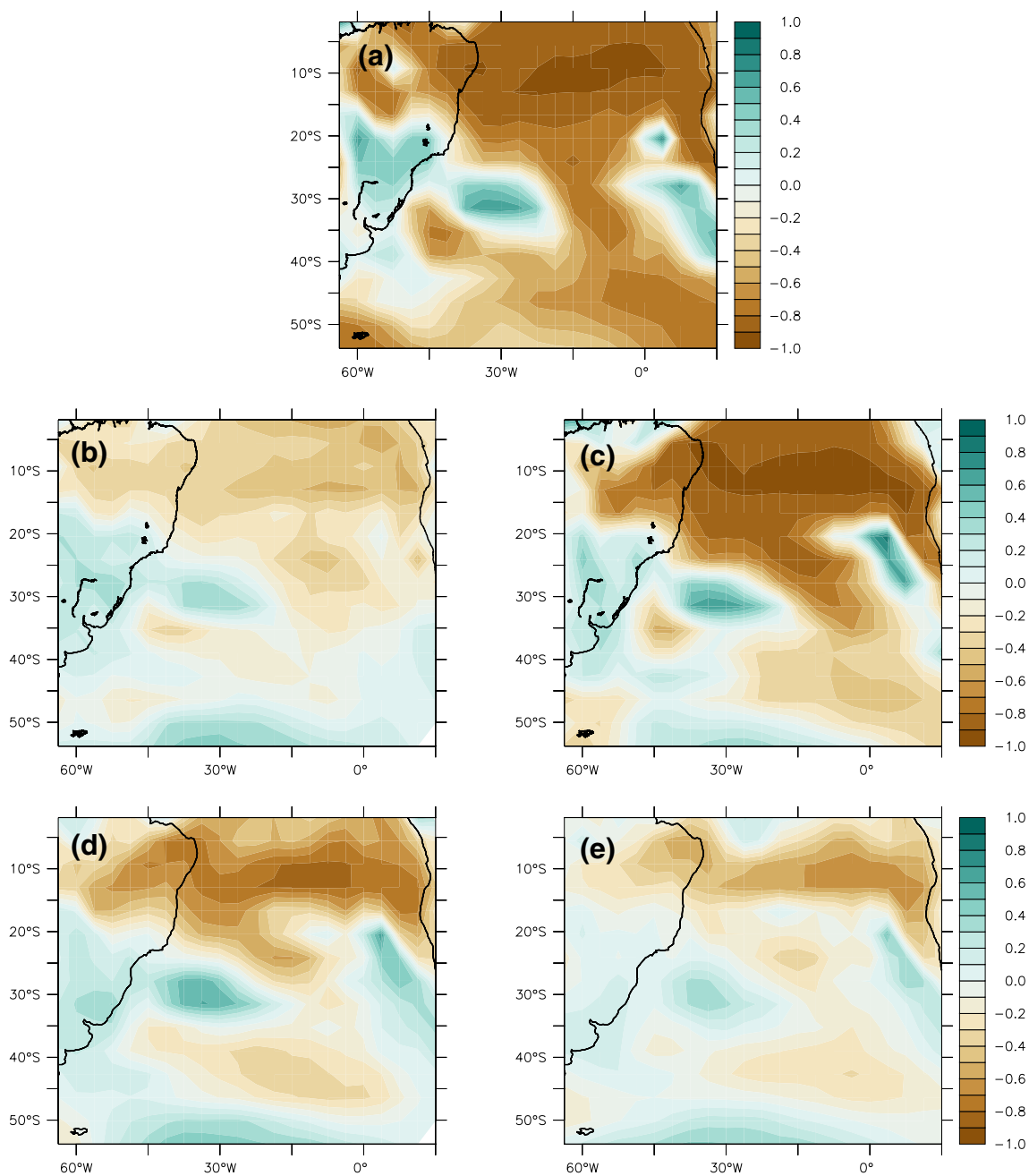


Fig. 8 Regression of the PPT field onto the SASD-index onto considering each of the five different climatic periods defined by the prescribed meltwater fluxes as in He (2011) and Marson et al. (2014):

a H1 (19 ka–14.67 ka); **b** BA/MWP1-A (14.67 ka–13.85 ka); **c** YD 12.9 ka–11.3 ka; **d** Early Holocene (11.3 ka–6 ka); **e** Late Holocene (6 ka–0)

4 Summary and conclusions

We followed-up on Wainer et al. (2014) that reconstructed from marine sediment data the SASD-index for the Holocene and related this index to changes in continental South American Precipitation. We use single forcing transient runs that considers individually varying forcings (e.g., meltwater, orbital, ice-sheets and greenhouse gases) to investigate the

changes of the SASD mode and its relationship to continental Northeast Brazil rainfall.

By evaluating the variability of rainfall connected to the SASD in the different climatic periods, here defined by the prescribed meltwater pulses, it was possible to differentiate what are the relative role of each individual forcing. In this way we could verify not only that the meltwater forcing is the predominant driver of SASD variability but also

the the assumption that rainfall changes are in fact related to changes in the South Atlantic SST-gradient and South Atlantic Northward heat transport.

We found that associated with a marked variability in the SASD-index induced by meltwater fluxes, the corresponding spatial patterns revealed that the SASD only acquires its observed configuration when all meltwater influx stops (Fig. 2). The role of meltwater becomes even more clearer when looking at the SASD-index wavelet spectrum obtained for the FULL forcing simulation results (Fig. 4a). The highest energy is at the lowest periods, coinciding with the timing of the cold events which is very similar to the wavelet spectrum pattern for the MWF results (Fig. 4b). There is very little energy in the higher periods, which would be the contribution of the other forcings (ORB, GHG and ICE) leaving no doubt with respect to the predominant role of meltwater in modulating the SASD.

A spatial distribution very similar to that seen for the evolution of the regression pattern of the SASD (Fig. 2) is recovered when the South Atlantic SST is regressed onto NEB-index (Fig. 5). This points to the connection between warming of the South Atlantic associated with the H1, YD and 8.2k prescribed large meltwater events. This is consistent with the results of McManus et al. (2004), that based on proxy records from marine sediments, show that during these cooling events the AMOC was weakened.

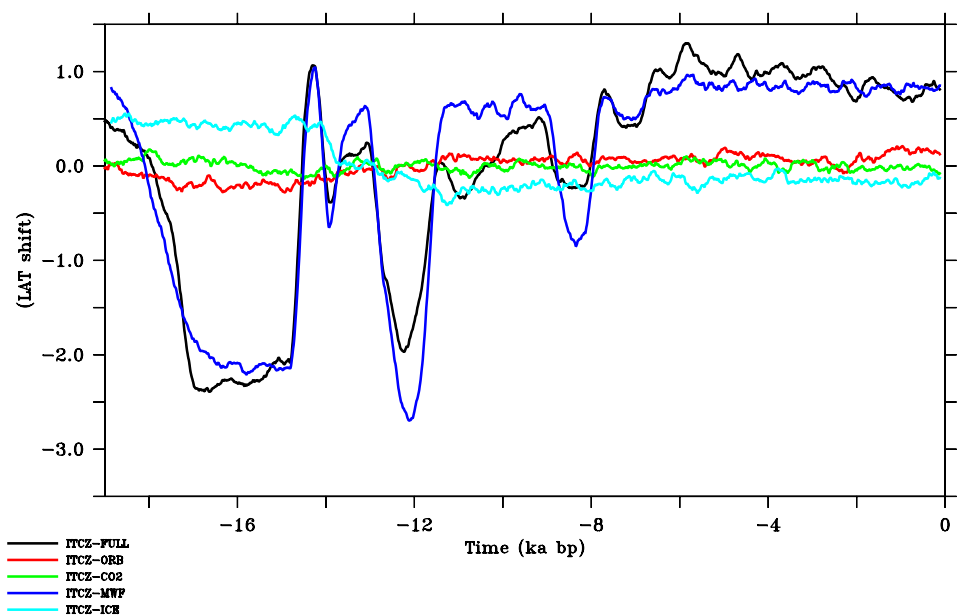
The evolution of the SASD spatial pattern, starting from the Northern Hemisphere cold events (H1 and YD), is related to the warming of the South Atlantic in response to the meltwater discharge. This is associated with the weakening of the Northward Heat transport and SST-gradient (Fig. 7). All these factors contribute to shifting the ITCZ south (Fig. 9).

The latitudinal position of the ITCZ in the Atlantic is obtained by locating when the meridional component of the wind-stress is zero ($\tau_y=0$) at 30° W and its shift is obtained by subtracting the mean. This is in agreement with Wanner et al. (2011), who discuss how the changes in energy distribution between Northern and Southern Hemisphere (due to changes in insolation) could lead to a southern shift of the ITCZ. It becomes clear that the southward shift of the ITCZ during the meltwater events since the last deglaciation is consistent with the variability of continental rainfall in northeast Brazil. The NEB-index shows increase in PPT with the warming of the South Atlantic driven by the weakened northward heat transport and South Atlantic SST-gradient that was shown in Fig. 6.

Wanner et al. (2011) discuss changes in interhemispheric energy distribution due to changes in insolation during the Holocene, and relate them with the Southern shift of the ITCZ. Here, we relate meltwater events with a reorganization of the AMOC and the transport of energy from the Southern to the Northern Hemisphere via ocean circulation. In other words, the interest is on how abrupt events can impact in the redistribution of energy through the AMOC response. Therefore, depending on the time scale of the phenomenon, one factor (e.g insolation) will prevail on the other (e.g northward heat transport and AMOC changes).

To further explore the relationship between the SASD and its impact on the ITCZ-related rainfall, wavelet spectral analysis was performed on the ITCZ latitudinal shift time-series (Fig. 9), for each of the runs. Figure 10 shows the wavelet power levels as a function of period and integration time where the same characteristics observed for the wavelet spectrum of the SASD-index is seen. The high energy at low frequencies (long periods, above ~ 3000 years) in the MWF

Fig. 9 Time series of the Latitudinal Shift of the ITCZ that is obtained when the meridional wind-stress is zero at 30° W. Southward shifts during the Northern Hemisphere cold events (H1, YD and the 8.2 k) are associated with an increase in NEB rainfall



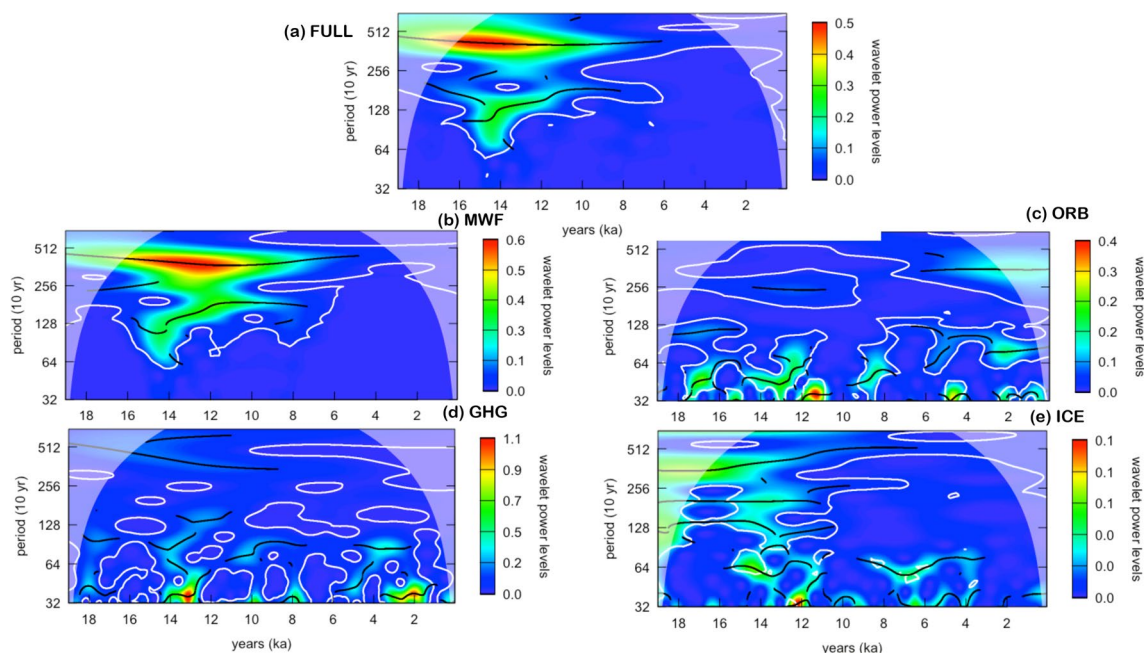


Fig. 10 Wavelet power levels for the ITCZ latitudinal shift time series (shown in Fig. 9) as a function of period for the integration time considering the simulation results of **a** FULL; **b** MWF; **c** ORB; **d** GHG and **e** ICE

forcing (Fig. 10b) is the predominant feature from 19 ka to about 11 ka in the FULL wavelet spectrum (Fig. 10a). This further confirms that meltwater discharges associated with the Northern Hemisphere cold events impact the latitudinal shift of the ITCZs, pushing it towards the NE pole of the SASD bringing more rain to NEB (c.c. Fig. 6). Energy in the wavelet spectrum of the ORB, GHG and ICE results (Fig. 10c–e, respectively) have little if any contribution for the spectrum in FULL (c.f. Fig. 10a), but it is interesting to note that the maximum power, for ORB, GHG and ICE are all around ~ 350 – 400 years, near the YD.

The investigation of the role of freshwater forcing on the overturning circulation in previous studies have shown that the increased freshwater in the North Atlantic is related to the reduced strength of the AMOC (e.g. Liu et al. 2015) and consequent warming of the Southern Hemisphere (e.g. Haskins et al. 2019; Brady and Otto-Bliesner 2011) and a southward shift of the ITCZ (Stouffer et al. 2006; Seo et al. 2014; McGee et al. 2014). Therefore, this work becomes particularly relevant because it associates the role of freshwater forcing affecting the strength of the Atlantic Meridional Overturning Circulation with changes in ocean heat transport and its relation to the dominant mode of climate variability in the South Atlantic having a direct impact on rainfall distribution. Nonetheless, changes in AMOC (or insolation) does not necessarily lead to development of the SASD, because the positive and negative SST anomaly poles require convergence and divergence of meridional heat transport, respectively.

Acknowledgements This study was supported in part by the Grants FAPESP: 2018/14789-9; CNPq: 301726/2013-2, 405869/20134; CNPq/MCT.INCT.CRIOSFERA 573720/20088 and Coordenação de Aperfeiçoamento de Pessoal de Nível Superior Brasil (CAPES) Finance Code 001 CAPES 88887.314387/2019-00, 88887.495715/2020-00. CNPq/MCT_INCT-CRIOSFERA 465680/2014.

References

- Addison PS (2018) Introduction to redundancy rules: the continuous wavelet transform comes of age
- Baker PA, Fritz SC (2015) Nature and causes of quaternary climate variation of tropical south america. *Quatern Sci Rev* 124:31–47
- Berger A (1978) Long-term variations of daily insolation and quaternary climatic changes. *J Atmos Sci* 35(12):2362–2367
- Brady EC, Otto-Bliesner BL (2011) The role of meltwater-induced subsurface ocean warming in regulating the atlantic meridional overturning in glacial climate simulations. *Clim Dyn* 37(7–8):1517–1532
- Buizert C, Keisling B, Box J, He F, Carlson A, Sinclair G, DeConto R (2018) Greenland-wide seasonal temperatures during the last deglaciation. *Geophys Res Lett* 45(4):1905–1914
- Cheng H, Fleitmann D, Edwards RL, Wang X, Cruz FW, Auler AS, Mangini A, Wang Y, Kong X, Burns SJ, et al (2009) Timing and structure of the 8.2 kyr bp event inferred from $\delta^{18}O$ records of stalagmites from China, Oman, and Brazil. *Geology* 37(11):1007–1010
- Clark PU, Shakun JD, Baker PA, Bartlein PJ, Brewer S, Brook E, Carlson AE, Cheng H, Kaufman DS, Liu Z et al (2012) Global climate evolution during the last deglaciation. *Proc Natl Acad Sci* 109(19):E1134–E1142
- Collins WD, Rasch PJ, Boville BA, Hack JJ, McCaa JR, Williamson DL, Briegleb BP, Bitz CM, Lin SJ, Zhang M (2006) The

- formulation and atmospheric simulation of the community atmosphere model version 3 (cam3). *J Clim* 19(11):2144–2161
- Deser C, Alexander MA, Xie SP, Phillips AS (2010) Sea surface temperature variability: Patterns and mechanisms. *Ann Rev Mar Sci* 2:115–143
- Green B, Marshall J, Donohoe A (2017) Twentieth century correlations between extratropical sst variability and itcz shifts. *Geophys Res Lett* 44(17):9039–9047
- Haskins RK, Oliver KI, Jackson LC, Wood RA, Drijfhout SS (2019) Temperature domination of amoc weakening due to freshwater hosing in two gcms. *Clim Dyn* pp 1–14
- Hastenrath S (2012) Exploring the climate problems of Brazil's nord-este: a review. *Clim Chang* 112(2):243–251
- Haug GH, Hughen KA, Sigman DM, Peterson LC, Röhl U (2001) Southward migration of the intertropical convergence zone through the holocene. *Science* 293(5533):1304–1308
- He F (2011) Simulating transient climate evolution of the last deglaciation with CCSM 3. PhD Thesis, University of Wisconsin
- He F, Shakun JD, Clark PU, Carlson AE, Liu Z, Otto-Bliesner BL, Kutzbach JE (2013) Northern hemisphere forcing of southern hemisphere climate during the last deglaciation. *Nature* 494(7435):81–85
- Joos F, Spahni R (2008) Rates of change in natural and anthropogenic radiative forcing over the past 20,000 years. *Proc Natl Acad Sci* 105(5):1425–1430
- Liu W, Liu Z, Cheng J, Hu H (2015) On the stability of the Atlantic meridional overturning circulation during the last deglaciation. *Clim Dyn* 44(5–6):1257–1275
- Liu Z, Otto-Bliesner B, He F, Brady E, Tomas R, Clark P, Carlson A, Lynch-Stieglitz J, Curry W, Brook E et al (2009) Transient simulation of last deglaciation with a new mechanism for bølling-allerød warming. *Science* 325(5938):310–314
- Liu Z, Carlson AE, He F, Brady EC, Otto-Bliesner BL, Briegleb BP, Wehrenberg M, Clark PU, Wu S, Cheng J et al (2012) Younger dryas cooling and the Greenland climate response to co2. *Proc Natl Acad Sci* 109(28):11101–11104
- Marson JM, Wainer I, Mata MM, Liu Z (2014) The impacts of deglacial meltwater forcing on the South Atlantic ocean deep circulation since the last glacial maximum. *Clim Past* 10(5):
- Marson JM, Mysak LA, Mata MM, Wainer I (2016) Evolution of the deep Atlantic water masses since the last glacial maximum based on a transient run of ncar-ccsm3. *Clim Dyn* 47(3–4):865–877
- Mayewski PA, Rohling EE, Stager JC, Karlén W, Maasch KA, Meeker LD, Meyerson EA, Gasse F, van Kreveld S, Holmgren K et al (2004) Holocene climate variability. *Quaternary Res* 62(3):243–255
- McGee D, Donohoe A, Marshall J, Ferreira D (2014) Changes in itcz location and cross-equatorial heat transport at the last glacial maximum, heinrich stadial 1, and the mid-holocene. *Earth Planet Sci Lett* 390:69–79
- McManus JF, Francois R, Gherardi JM, Keigwin LD, Brown-Leger S (2004) Collapse and rapid resumption of Atlantic meridional circulation linked to deglacial climate changes. *Nature* 428(6985):834–837
- Moreno-Chamarro E, Marshall J, Delworth T (2020) Linking itcz migrations to the amoc and North Atlantic/pacific sst decadal variability. *J Clim* 33(3):893–905
- Morioka Y, Tozuka T, Yamagata T (2011) On the growth and decay of the subtropical dipole mode in the south atlantic. *J Clim* 24(21):5538–5554
- Morioka Y, Tozuka T, Masson S, Terray P, Luo JJ, Yamagata T (2012) Subtropical dipole modes simulated in a coupled general circulation model. *J Clim* 25(12):4029–4047
- Moura AD, Shukla J (1981) On the dynamics of droughts in Northeast Brazil: observations, theory and numerical experiments with a general circulation model. *J Atmos Sci* 38(12):2653–2675
- Mulitza S, Chiessi CM, Schefuß E, Lippold J, Wichmann D, Antz B, Mackensen A, Paul A, Prange M, Rehfeld K et al (2017) Synchronous and proportional deglacial changes in Atlantic meridional overturning and Northeast Brazilian precipitation. *Paleoceanography* 32(6):622–633
- Nnamchi HC, Li J, Anyadike RN (2011) Does a dipole mode really exist in the South Atlantic ocean? *J Geophys Res Atmos* 116(D15)
- O'brien S, Mayewski PA, Meeker LD, Meese DA, Twickler MS, Whitlow S (1995) Complexity of Holocene climate as reconstructed from a Greenland ice core. *Science* 270(5244):1962–1964
- Otto-Bliesner BL, Brady EC, Clauzet G, Tomas R, Levis S, Kothavala Z (2006) Last glacial maximum and Holocene climate in ccsm3. *J Clim* 19(11):2526–2544
- Peltier W (2004) Global glacial isostasy and the surface of the ice-age earth: the ice-5g (vm2) model and grace. *Annu Rev Earth Planet Sci* 32:111–149
- Portilho-Ramos R, Chiessi C, Zhang Y, Mulitza S, Kucera M, Sicha M, Prange M, Paul A (2017) Coupling of equatorial Atlantic surface stratification to glacial shifts in the tropical rainbelt. *Sci Rep* 7(1):1–8
- Ruddiman W, Fuller D, Kutzbach J, Tzedakis P, Kaplan J, Ellis E, Vavrus S, Roberts C, Fyfe R, He F et al (2016) Late Holocene climate: natural or anthropogenic? *Rev Geophys* 54(1):93–118
- Seo J, Kang SM, Frierson DM (2014) Sensitivity of intertropical convergence zone movement to the latitudinal position of thermal forcing. *J Clim* 27(8):3035–3042
- Servain J (1991) Simple climatic indices for the tropical Atlantic ocean and some applications. *J Geophys Res Oceans* 96
- Stouffer RJ, Yin J, Gregory J, Dixon K, Spelman M, Hurlin W, Weaver A, Eby M, Flato G, Hasumi H et al (2006) Investigating the causes of the response of the thermohaline circulation to past and future climate changes. *J Clim* 19(8):1365–1387
- Stríkis NM, Chiessi CM, Cruz FW, Vuille M, Cheng H, de Souza Barreto EA, Mollenhauer G, Kasten S, Karmann I, Edwards RL et al (2015) Timing and structure of mega-Sacz events during Heinrich stadial 1. *Geophys Res Lett* 42(13):5477–5484A
- Stríkis NM, Cruz FW, Barreto EA, Naughton F, Vuille M, Cheng H, Voelker AH, Zhang H, Karmann I, Edwards RL et al (2018) South American monsoon response to iceberg discharge in the north Atlantic. *Proc Natl Acad Sci* 115(15):3788–3793
- Taschetto AS, Wainer I et al (2008) The impact of the subtropical South Atlantic sst on South American precipitation. *Ann Geophys Atmos Hydrospheres Space Sci* 26(11):3457
- Tierney JE, Pausata FS, de Menocal PB (2017) Rainfall regimes of the green sahara. *Sci Adv* 3(1):e1601,503
- Torrence C, Compo G (1998) A practical guide to wavelet analysis. *Bull Am Meteorol Soc* 79(1):61–78
- Wainer I, Soares J (1997) North Northeast Brazil rainfall and its decadal-scale relationship to wind stress and sea surface temperature. *Geophys Res Lett* 24(3):277–280
- Wainer I, Venegas SA (2002) South Atlantic multidecadal variability in the climate system model. *J Clim* 15(12):1408–1420
- Wainer I, Prado L, Khodri M, Otto-Bliesner B (2014) Reconstruction of the South Atlantic subtropical dipole index for the past 12,000 years from surface temperature proxy. *Sci Rep* 4:5291
- Walker M, Head MJ, Lowe J, Berkelhammer M, Björck S, Cheng H, Cwynar LC, Fisher D, Gkinis V, Long A et al (2019) Subdividing the Holocene series/epoch: formalization of stages/ages and subseries/subepochs, and designation of gssps and auxiliary stratotypes. *J Quat Sci* 34(3):173–186
- Wanner H, Solomina O, Grosjean M, Ritz SP, Jetel M (2011) Structure and origin of Holocene cold events. *Quat Sci Res* 30(21–22):3109–3123
- Weaver AJ, Saenko OA, Clark PU, Mitrovica JX (2003) Meltwater pulse 1a from Antarctica as a trigger of the Bølling–Allerød warm interval. *Science* 299(5613):1709–1713

- Wen X, Liu Z, Wang S, Cheng J, Zhu J (2016) Correlation and anti-correlation of the East Asian summer and winter monsoons during the last 21,000 years. *Nat Commun* 7(1):1–7
- Yeager SG, Shields CA, Large WG, Hack JJ (2006) The low-resolution ccsm3. *J Clim* 19(11):2545–2566

Publisher's Note Springer Nature remains neutral with regard to jurisdictional claims in published maps and institutional affiliations.